Salt bridge-forming residues positioned over viral peptides presented by MHC class I impacts T-cell recognition in a binding-dependent manner

Wei Ji[a],[1], Ling Niu[b],[1], Weiyu Peng[a], Yongli Zhang[c], Hao Cheng[d], Feng Gao[e], Yi Shi[b], Jianxun Qi[a], George F. Gao[a],[b],[d],[*], William J. Liu[a],[c],[*]

[a] NHC Key Laboratory of Medical Virology and Viral Diseases, National Institute for Viral Disease Control and Prevention, Chinese Center for Disease Control and Prevention, Beijing 100052, China
[b] CAS Key Laboratory for Pathogenic Microbiology and Immunology, Chinese Academy of Sciences, Beijing 100101, China
[c] School of Laboratory Medicine and Life Sciences, Wenzhou Medical University, Wenzhou, China
[d] Research Network of Immunity and Health (RNIH), Beijing Institutes of Life Science, Chinese Academy of Sciences, Beijing 100101, China
[e] Institute of Genetics and Developmental Biology, Chinese Academy of Sciences, Beijing, China

ABSTRACT

The viral peptides presentation by major histocompatibility complex class I (MHC I) molecules play a pivotal role in T-cell recognition and the subsequent virus clearance. This process is delicately adjusted by the variant residues of MHC I, especially the residues in the peptide binding groove (PBG). In a series of MHC I molecules, a salt bridge is formed above the N-terminus of the peptides. However, the potential impact of the salt bridge on peptide binding and T-cell receptor (TCR) recognition of MHC I, as well as the corresponding molecular basis, are still largely unknown. Herein, we determined the structures of HLA-B*4001 and H-2K^d in which two different types of salt bridges (Arg62-Glu163 or Arg66-Glu163) across the PBG were observed. Although the two salt bridges led to different conformation shifts of both the MHC I α helix and the peptides, binding of the peptides with the salt bridge residues was relatively conserved. Furthermore, through a series of *in vitro* and *in vivo* investigations, we found that MHC I mutations that disrupt the salt bridge alleviate peptide binding and can weaken the TCR recognition of MHC I-peptide complexes. Our study may provide key references for understanding MHC I-restricted peptide recognition by T-cells.

1. Introduction

The presentation of viral peptides to host T lymphocytes is crucial for adaptive cellular immunity to clear viruses during the infection. In the structures of MHC I presenting these short peptides, the α1 and α2 domains of MHC I form a bed-like groove to comfortably accommodate the peptides: two α-helices as the bedrails and the β-sheets beneath as the mattress (Bjorkman et al., 1987; Niu et al., 2013). The short peptides interact with the amino acids within the peptide binding groove (PBG) through different binding modes. First, the featured residues at the second position (P2) from the N-terminus and the last residue (PΩ) at the C-terminus of the peptides, termed primary anchor residues, protrude into the specific pockets in the PBG of the MHC I. Though the positions of the primary anchors on the peptides are relatively conserved, the binding modes of the anchoring residues of the peptides to

different MHC I molecules are diversified due to polymorphisms in the pocket-forming residues. Second, the peptides also interact with the PBG *via* contacts between the backbone atoms of the peptides and the PBG residues (Mitaksov and Fremont, 2006). Third, a hydrogen bond network is formed between the two termini of the peptides and the conserved residues in the PBG. The latter two interaction modes are relatively conserved between different MHC I molecules (Fremont et al., 1992; Madden et al., 1993).

Generally, MHC I binding peptides are located in the bottom of a ringent PBG, which leaves a solvent-exposed top surface of the entire peptide from the N- to the C-terminus, ready for the recognition of the T-cell receptors (TCR) (Bjorkman et al., 1987). However, based on the structures of a series of MHC I molecules, such as human HLA-B*2705 (Madden et al., 1991), rhesus macaque Mamu-A*02 (Liu et al., 2011), and mouse H-2K^d (Mitaksov and Fremont, 2006; Zhou et al., 2004),

there is a salt bridge positioned over the peptides formed by opposite charged residues from the α1 and α2 helices of MHC I, respectively. In humans and macaques, the salt bridge is formed by the positively charged Arg62 on the α1 helix and the negatively charged Glu163 on the α2 helix. Meanwhile, in mice, the involved residues are Arg66 on α1 helix and Glu163 on α2 helix. Both of these types of salt bridges overhang the N-terminal portion of the T-cell epitopes in the groove. Obviously, the salt bridge forms a ligature to tightly fix the peptides into the PBG. However, thus far, it is still largely unknown how the formation of these salt bridges in MHC I molecules impacts peptide binding.

Further, considering that these salt bridges are also solvent-exposed, they are in the position to be recognized by TCRs. Generally, T-cell activation by the MHC-peptide complex may occur in three correlated ways: 1) direct interaction of the TCR with the MHC, termed MHC restriction; 2) direct interaction of the TCR with the solvent-accessible peptide main chain and side chains; and 3) interaction of the peptide with the TCR mediated by conformational perturbations in the MHC-peptide complex (Baker et al., 2012; Gras et al., 2012). Crystallographic studies clearly demonstrate that the polymorphic amino acids in the grooves of MHC I molecules from different mammals may influence the peptide conformation, subsequently impacting T-cell recognition (Borbulevych et al., 2009; Hulsmeyer et al., 2004; Insaidoo et al., 2011). Nevertheless, to our knowledge, it has not been determined if the salt bridges in some MHC I molecules impact TCR recognition through a direct interaction with the TCR or indirectly through modulation of the peptide conformation.

Herein, by determining the crystal structures of human MHC I HLA-B*4001 complexed with a severe acute respiratory syndrome coronavirus (SARS-CoV) nucleocapsid (*N*)-derived T-cell epitope (Oh et al., 2011) and mouse MHC I H-2K^d bound to an immunodominant T-cell epitope from human hepatitis B virus (HBV) core antigen (HBc) (Li et al., 2005), we clearly demonstrated the molecular features of MHC I molecules with two different salt bridges formed by the residues pairs Arg62-Glu163 and Arg66-Glu163, respectively. We further investigated the impacts of the salt bridges on peptide binding and T-cell recognition by constructing a series of MHC I mutants *in vitro* and *in vivo*. Our results elucidated the key features of mammalian MHC I molecules with salt bridges in the PBG and will benefit T-cell based diagnosis and vaccine development.

2. Materials and methods

2.1. Peptide synthesis and preparation of expression constructs

The human HBV HBc protein-derived peptide HBc87-95 (SYVNTNMGL) (Li et al., 2005) and SARS-CoV N protein-derived peptide N216-225 (GETALALLLL) (Oh et al., 2011) were synthesized with 95% purity by reverse-phase high performance liquid chromatography (SciLight Biotechnology, Beijing, China). The peptides were stored at −80 °C as freeze-dried powders and were dissolved in dimethyl sulfoxide before use. The expression plasmid for mouse MHC I H-2K^d was constructed previously in our lab (Zhou et al., 2004). We also constructed three H-2K^d salt bridge mutants (R66A, E163A, and R66A&E163A) and three control mutants (S69A, R157A, A158 G) based on the WT plasmid (GENEWIZ). For the HLA-B*4001 expression construct, the gene (GenBank Q04826) was synthesized and ligated into the pET21a vector (Shanghai Generay). The three HLA-B*4001 salt bridge mutants (R62A, E163A, R62A&E163A) and three control mutants (I66A, R157A, A158 G) were also constructed on the basis of the WT construct.

2.2. Mice

Six- to eight-week-old female BALB/c mice were purchased from Vital River Laboratory Animal Technology Company (Beijing, China) and raised under specific pathogen-free conditions. All experiments were performed in strict compliance with the Guide for the Care and Use of Laboratory Animals of the People's Republic of China and approved by the Committee on the Ethics of Animal Experiments of National Institute for Viral Disease Control and Prevention, Chinese Center for Disease Control and Prevention.

2.3. Vaccine immunization

Mice in the experimental group were subcutaneously injected at multiple sites with HBV peptide HBc87-95 and the N-terminal fragment N333 (23–355aa) of murine gp96 emulsified in complete Freund's adjuvant for the first dose. Mice were administered the mixture of peptide, gp96 fragment, and incomplete Freund's adjuvant twice in 2-week intervals for the next two doses. Mice were sacrificed to harvest splenocytes on Day 7 after the final immunization. Mice in the control group were immunized with a mixture of phosphate buffered saline (PBS), gp96 fragment, and Freund's adjuvant.

2.4. ELISPOT assays

Antigen-specific T lymphocyte responses were detected with an IFN-γ-secreting ELISPOT assay by using splenocytes as previously described (Tan et al., 2017). Briefly, 96-well plates were coated with 100 μL/well of 5 mg/mL anti-mouse IFN-γ antibody (BD Pharmingen, San Diego, CA) overnight at 4 °C. After washing with PBS twice, the plates were blocked with culture medium for 2 h at room temperature. Mouse spleens were ground and filtered through cell strainers. Cells were processed with red blood cell lysis buffer (0.144 M NH$_4$Cl and 17 μM Tris, pH 7.2). We washed cells with PBS twice and centrifuged them to harvest lymphocytes. Fresh mouse splenocytes (2.5×10^5) in 100 μL Roswell Park Memorial Institute (RPMI) 1640 medium with 10% fetal bovine serum (FBS) were seeded in each well. Then, the peptides (10 μg/mL) were added to the wells and incubated at 37 °C in 5% CO$_2$ for 18 h. Phytohaemagglutinin (PHA) was added as the positive control for nonspecific stimulation. Cells incubated with medium alone were employed as a negative control that produced less than five spots in 90% of the experiments. Finally, the cells were removed, and the plates were processed according to the manufacturer's instructions (BD). The colored spots, which represent epitope-specific T-cells, were counted and analyzed using an automatic ELISPOT reader (CTL Corp.).

2.5. Refolding and purification of MHC class I

Murine MHC class I H-2K^d and β$_2$m or human MHC class I HLA-B*4001 heavy chain and human β$_2$m were overexpressed in *Escherichia coli* as inclusion bodies and subsequently refolded *in vitro* in the presence of a high concentration of peptide, as described previously (Xiao et al., 2016). Briefly, the dissolved MHC I heavy chain and β$_2$m inclusion body and peptides were diluted at a molar ratio of 1:1:3, respectively, in refolding buffer (100 mM Tris−HCl, 400 mM L-arginine, 2 mM EDTA-Na, 5 mM Glutathione [GSH], and 0.5 mM L-Glutathione oxidized [GSSG]). After 12 h of slow stirring at 4 °C, the MHC I/peptide complex was then concentrated and purified *via* Superdex 200 10/300 G L (GE Healthcare) chromatography.

2.6. Tetramer preparation and flow cytometry

WT H-2K^d and the three H-2K^d mutant-restricted tetramers of HBV-peptide were prepared as previously described (Liu et al., 2012a; Zhang et al., 2018; Zhou et al., 2006). Briefly, recombinant H-2K^d/peptide complexes were purified and then biotinylated by incubation with D-biotin, ATP, and the biotin protein ligase BirA (Avidity) at 4 °C for 12 h. The biotinylated H-2K^d was further purified by gel filtration to remove free biotin, and then the multimers were produced by using PE-streptavidin (Sigma). Cells from the subjects were stained with PE-tetramer and FITC-conjugated anti-CD8 antibody. All samples were analyzed

Table 1
X-ray diffraction data processing and refinement.

Data	HLA-B*4001	H-2K^d
Data processing		
Space group	P2$_1$2$_1$2$_1$	P2$_1$2$_1$2$_1$
Cell parameters		
a (Å)	52.48	89.082
b (Å)	69.27	110.398
c (Å)	120.94	47.015
α (°)	90	90
β (°)	90	90
γ (°)	90	90
Resolution range(Å)	50-2.30(2.38-2.3)^a	50-2.06(2.08-2.04)
Total reflections	141128	236416
Unique reflections	19343	29503
Completeness (%)	99.9(100)	99.9(100)
R_{sym} (%)	9.8(43.7)	7.9(37.9)
I/σ	20.26(4.89)	28.5(8.1)
Refinement		
R_{work} (%)	21	19
R_{free} (%)	26	24.1
RMSD		
Bond lengths(Å)	0.006	0.0072
Bond angles (°)	0.917	0.84
Ramachandran plot quality		
Most favored (%)	89.9	96
allowed (%)	10.1	4
Disallowed (%)	0	0

RMSD, root mean square deviation.

[a] Values in parentheses are given for the highest resolution shell.

with a FACSCalibur flow cytometer (BD Biosciences) after staining.

2.7. X-ray crystallography, structure determination, and refinement

The conditions for the protein purification and the crystal growth of the complex formed by H-2K^d with HBV peptide HBc87-95 was described previously (Zhou et al., 2004). Human β$_2$m was used to generate the H-2K^d/HBc87-95 complex. The renatured HLA-B*4001/N216-225 complex was further purified by Resource Q anion-exchange chromatography before crystallization. Crystallization was performed using the hanging drop vapor diffusion technique. The concentration of protein was 12 mg/mL, and the crystals grew in 0.1 M sodium citrate tribasic dehydrate (pH 6.5) and 18% (w/v) polyethylene glycol 3350 at 4 °C. For cryoprotection, crystals were transferred to reservoir solutions containing 15% glycerol, flash-cooled, and maintained at 100 K in a stream. X-ray diffraction data were collected at 100 K at the SSRF BEAMLINE BL17U (Shanghai, China) at a wavelength of 0.97907 Å (Table 1). The structure of H-2K^d/HBc87-95 and HLA-B*4001/N216-225 were resolved through the molecular replacement method using the MHC I structures with PDB codes 1FG2 and 4F7M, respectively (Liu et al., 2012b) as the model in the Crystallography and NMR System (CNS) program. Detailed model building was performed by hand using COOT, and restrained refinement was performed using REFMAC5. The stereochemical quality of the final model was assessed with the program PROCHECK. Structure-related figures were processed by PyMOL.

2.8. Determination of complex thermostability using CD spectroscopy

To evaluate the thermostability of different MHC I complexes and also their mutants, we used CD spectroscopy as previously described (N. Zhang et al., 2011). We repeated at least three times for each protein. All complexes were prepared as described above and diluted to 0.2 mg/mL in 20 mM Tris−HCl (pH 8.0) and 50 mM NaCl. Thermal denaturation curves were determined by monitoring the CD value at 218 nm using a 1-mm optical path-length cell as the temperature was raised from 20 to 100 °C at a rate of 1 °C/min. The temperature of the sample solution was directly measured with a thermistor. The fraction of unfolded protein was calculated from the mean residue ellipticity (θ) by the standard method. The unfolded fraction (%) is expressed as (θ - θ$_N$) / (θ$_U$ - θ$_N$), where θ$_N$ and θ$_U$ are the mean residue ellipticity values in the fully folded and fully unfolded states, respectively. The midpoint transition temperature (T_m) was determined by fitting the data to the denaturation curves using the Origin 8.0 program (OriginLab).

2.9. Statistical analysis

For comparisons between multiple groups, two-way ANOVA with Bonferroni post-tests was performed. One-way ANOVA analysis with Bonferroni post-tests was used for comparison between multiple columns. Statistical significance of differences between two columns was determined by Student's *t*-test All tests were two-tailed with a significance level of 0.05. All data analyses were performed with GraphPad Prism.

2.10. Protein structure accession numbers

The coordinates and structure factors of SARS-CoV peptide N216-225 complexed to HLA-B*4001 and HBV peptide HBc87-95 complexed to H-2K^d have been deposited in the PDB under accession numbers 6IEX and 1VGK, respectively.

3. Results

3.1. The salt bridge formation across the peptide binding groove of MHC I is substantial in different vertebrates

The retrieval of the MHC I protein sequences available in the IPD-MHC Database (https://www.ebi.ac.uk/ipd/mhc/) showed that 12%–26% of the MHC I alleles available possess the paired residues for the potential salt bridge formation (Table 2). The Type 1 salt bridge is formed by R66 on the α1-helix and E163 on the α2-helix, such as in H-2K^d, while the Type 2 salt bridge is constructed by R62 and E163 on the α1- and α2-helices, respectively, such as in HLA-B*4001.

Moreover, we retrieved the allele frequency of MHC I molecules which are confirmed to possess salt bridge from the crystal structures in

Table 2
The statistics of potential salt bridges in the MHC I molecules of different vertebrates[a].

Species	Latin	Total alleles	R66	R62	E163	R66 E163	R62 E163	PCT[b]
Human	*Homo sapiens*	3989	0	3096	485	0	472	12%
Non-Human Primates	*Macaca fascicularis*	247	48	89	102	23	41	26%
Murids	*Rattus norvegicus*	31	3	17	7	2	5	23%
Suids	*Sus scrofa*	57	2	37	10	0	10	18%
Bovins	*Bos taurus*	77	9	51	18	0	12	16%
Ovids	*Ovis aries*	23	2	15	6	0	3	13%
Salmonids	*Salmo salar*	48	0	18	16	0	6	13%

[a] Data retrived from Immuno Polymorphism Database (https://www.ebi.ac.uk/ipd/mhc/).
[b] PCT, percentage.

population in The Allele Frequency Net Database (http://www.allelefrequencies.net/default.asp). HLA-B*4001, HLA-B*4002 and HLA-B*0702-carrying population distributed widely in American, Asian and European Continents (Table S1), with the highest frequency (29%) of HLA-B*4001 in American Samoa, 27.6% HLA-B*4002 in Australia Kimberly Aborigine and 17.60% HLA-B*0702 in Ireland South. Thus, these three HLA alleles possessing Type 2 salt bridge (R62&E163) were popular among the populations with different ethnics. In addition to HLA alleles, among the MHC I alleles of the rhesus macaque, Mamu A*02 which possesses Type 2 salt bridge is prevalent, presenting in > 20% of macaques (Liu et al., 2011). The allele H-2K^d with Type 1 salt bridge is also common in mouse MHC alleles. Thus, the impacts of the salt bridge formation overhead the PBG on the peptide binding and recognition by TCR would be a substantial phenomenon for different vertebrates, which has emerged in fish.

3.2. The binding capacity of MHC I to peptides is influenced by the salt bridges

To determine the potential role of the MHC I salt bridge in peptide binding, we utilized the peptide HBc87-95 to facilitate the *in vitro* renaturation of H-2K^d and its salt bridge mutants H-2Kd-M1(Mutant R66A), H-2Kd-M2 (Mutant E163A), and H-2Kd-M3 (Mutant R66A& E163A) followed by size exclusion chromatography (gel filtration) analyses. The control mutants H-2Kd-C1 (Mutant R157A), H-2Kd-C2 (Mutant A158G), H-2Kd-C3 (Mutant S69A), which preserve the salt bridge were proceeded the same experiment as control mutants. Compared to wild type (WT) of H-2K^d, all the three salt bridge mutants generated relatively lower yields of refolded products at the size

expected for an MHC I monomer. However, the control mutants showed similar yields of renatured products as WT H-2K^d (Fig. 1A and Table S2).

The binding stabilities of the peptide HBc87-95 with H-2K^d and all the mutants were further analyzed by circular dichroism (CD) spectroscopy (Fig. 1B), with the T_ms determined from melting curves. WT H-2K^d complexed with the HBc87-95 peptide was stable, with a T_m of 87.3 ± 2.3 °C. As expected, the H-2K^d salt bridge mutants H-2Kd-M1, H-2Kd-M2, and H-2Kd-M3 displayed significantly decreased stability with lower T_ms (81.3 ± 0.5 °C for H-2Kd-M1, 78.5 ± 3.8 °C for H-2Kd-M2, and 80.4 ± 0.5 °C for H-2Kd-M3). Moreover, the T_ms of the control mutants have no statistically differences with WT H-2K^d (87.8 ± 0.4 °C for H-2Kd-C1, 88.2 ± 0.3 °C for H-2Kd-C2, 87.8 ± 0.3 °C for H-2Kd-C3).

We also determined the binding capacity of the SARS-CoV-derived peptide N216-225 with the human MHC I HLA-B*4001, and its salt bridge mutants B4001-M1 (Mutant R62A), B4001-M2 (Mutant E163A), and B4001-M3 (Mutant R62A&E163A) and its control mutants B4001-C1 (Mutant A158 G), B4001-C2 (Mutant R157A), B4001-C3 (Mutant I66A). We found that three salt bridge mutants B4001-M1 (84.2 ± 0.4 °C), B4001-M2 (82.8 ± 0.7 °C), and B4001-M3 (82.9 ± 0.7 °C) displayed significantly lower binding capacity for the peptide compared to WT HLA-B*4001(85.9 ± 0.6 °C) (Fig. 1C and 1D), while the control mutants showed the identical binding capacity with the peptides as WT HLA-B*4001 (Fig.1C and 1D). Thus, the salt bridge formation in both PBGs of H-2K^d and HLA-B*4001 contributed to the binding of the peptides, though breaking the salt bridge did not abolish peptide binding.
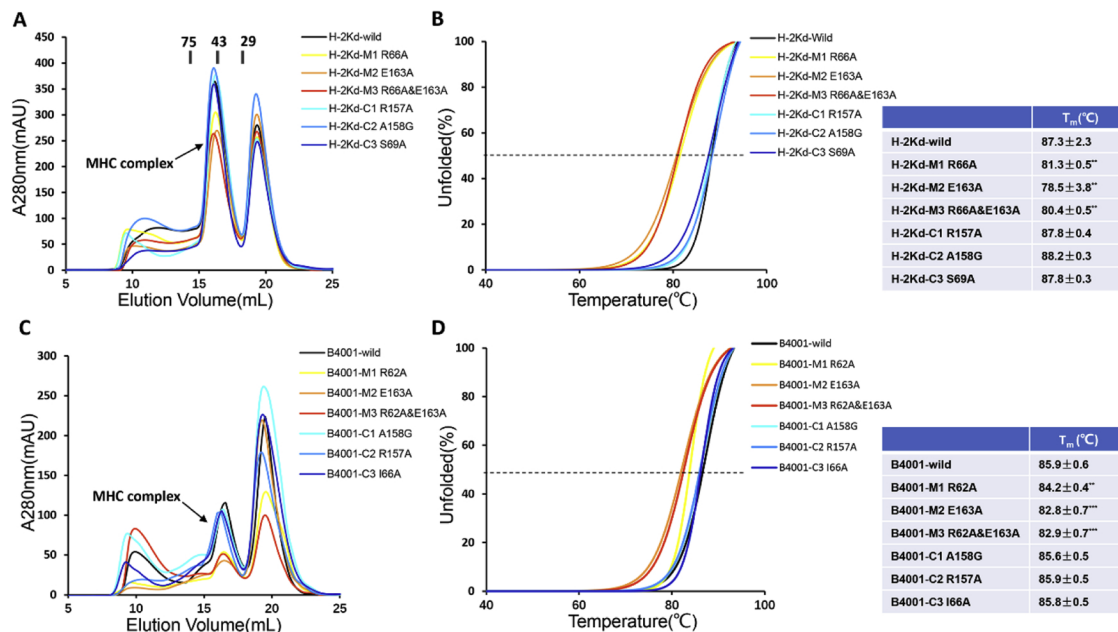

Fig. 1. The impact of MHC I salt bridges on peptide binding capacity.
(**A**) Binding of human hepatitis B virus (HBV) core antigen-derived immunodominant T-cell epitope HBc87-95 to H-2K^d, its three salt bridge mutants (H-2Kd-M1: Mutant R66A, H-2Kd-M2: Mutant E163A and H-2Kd-M3: Mutant R66A&E163A) and three control mutants (H-2Kd-C1:Mutant R157A, H-2Kd-C2:Mutant A158 G and H-2Kd-C3:Mutant S69A) by *in vitro* refolding. The absorbance peak of the H-2K^d complex with the expected molecular mass of 45 kDa was eluted at the estimated volume of 16 mL on a Superdex 200 10/300 G L column. The profile is marked with approximate positions of the molecular mass standards of 75.0, 43.0, and 29.0 kDa. The blue colors in different shades represent the three control mutants, and the yellow, orange, red represent three salt bridge mutants, respectively. (**B**) Thermostability of peptide HBc87-95 complexed to H-2K^d and its mutants by CD spectroscopy. The T_ms of different complexes are indicated by the temperature when 50% of the protein unfolded at the black dashed line. We repeated CD at least three times for each protein, the results were showed by mean ± SD, Statistical significance of differences between the wild and mutant was determined by student's t test. **, $P < 0.01$; ***, $P < 0.001$. (**C**) HLA-B*4001, its three salt bridge mutants (B4001-M1: Mutant R62A, B4001-M2: Mutant E163A, and B4001-M3: Mutant R62A&E163A) and three control mutants (B4001-C1: Mutant A158 G, B4001-C2: Mutant R157A and B4001-C3: Mutant I66A) complexed to severe acute respiratory syndrome coronavirus (SARS-CoV) nucleocapsid (*N*)-derived T-cell epitope N216-225 were refolded *in vitro*. (**D**) Thermostability of HLA-B*4001 and its mutants as measured by CD spectroscopy. (For interpretation of the references to colour in this figure legend, the reader is referred to the web version of this article).
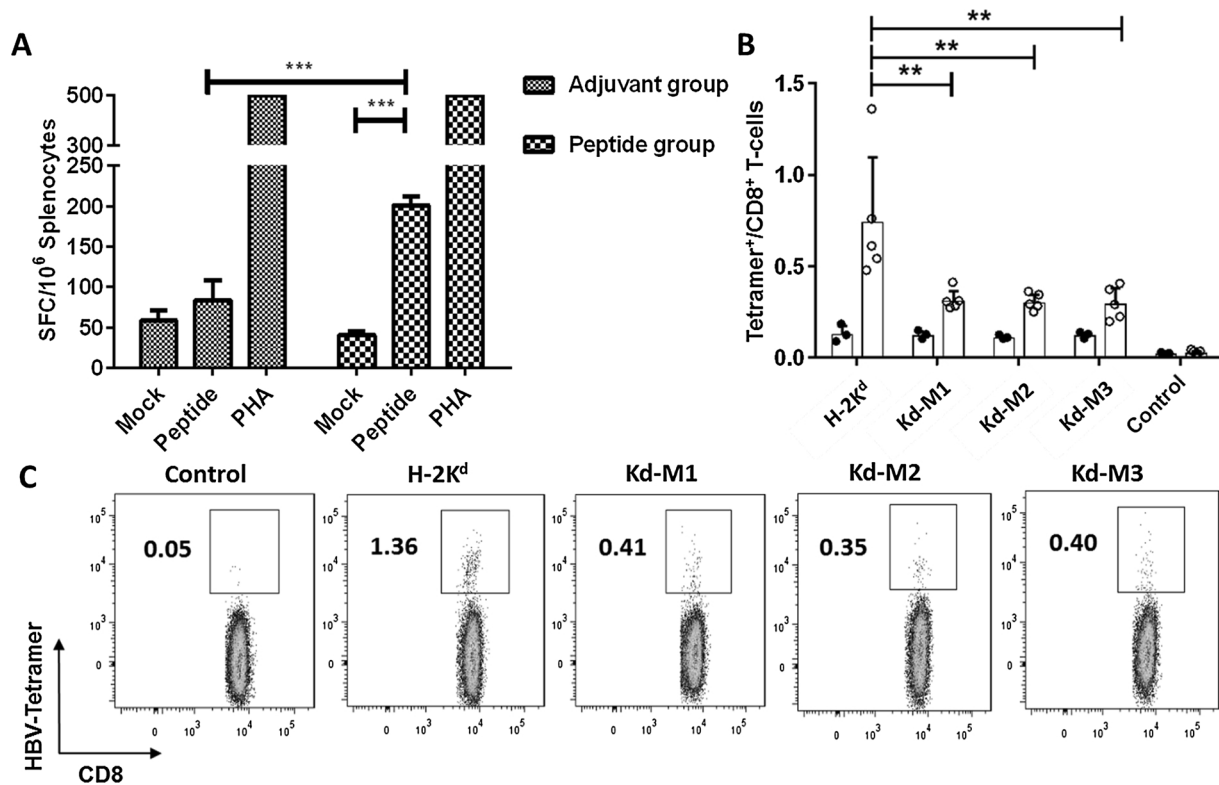
Fig. 2. T-cell recognition of the salt bridge residues of MHC I.
(**A**) Mouse T-cell immune responses induced by human hepatitis B virus (HBV) core antigen-derived T-cell epitope HBc87-95. The Balb/c mice were immunized with HBc87-95 peptide (Peptide group) or PBS (Adjuvant group) together with adjuvants. ELISPOT assays were performed using freshly isolated mouse splenocytes. The non-specific stimulant PHA was used as a positive control, and mock indicates the negative control without any stimulant. (**B**) Peptide-specific CD8$^+$ T-cells stained by tetramers of H-2K^d and mutants. The HBc87-95 peptide-specific CD8$^+$ T-cells in the freshly isolated splenocytes from vaccinated mice were stained by H-2K^d tetramer, Kd-M1 (Mutant R66A) tetramer, Kd-M2 (Mutant E163A) tetramer, and Kd-M3 (Mutant R66A&E163A)tetramer, respectively. The hollow dots represent the peptide-immunized group, and the black dots represent the adjuvant group. The control was staining with unrelated tetramer (HLA-A2/influenza peptide GL9). Error bars represent means ± SD. n = 5 mice for per peptide group, n = 3 mice for per adjuvant group. (**C**) The representative peptide-specific CD8$^+$ T-cells stained by tetramers of H-2K^d and mutants. The statistical analysis between two groups used two-way ANOVA with Bonferroni post-tests. ** $p < 0.01$, *** $p < 0.001$.

3.3. The impact of the salt bridge on the T-cell recognition

To further investigate the role of the MHC I salt bridge above the PBG in T-cell recognition, we established a mouse model *via* three rounds of fortnightly *in vivo* injection of the HBV-derived peptide HBc87-95. ELISPOT assays were then performed using freshly isolated splenocytes to assess the T-cell immune responses induced by the peptide. No specific reactivity of IFN-γ secretion could be detected in splenocytes separated from placebo-immunized mice (< 10 SFCs/10^5 splenocytes). In contrast, CD8$^+$ T-cells from splenocytes of the mice immunized with peptide HBc87-95 presented strong IFN-γ production (Fig. 2A). The splenocytes from the peptide-inoculated mice were also stained with the H-2K^d tetramers prepared in the presence of peptide HBc87-95. The splenocytes from HBc87-95-inoculated mice contained $0.75 \pm 0.36\%$ of peptide-specific CD8$^+$ T-cells (Fig. 2B and C). No peptide-specific CD8$^+$ T-cells were identified from splenocytes of mice inoculated with placebo, as judged by HBc87-95 tetramer staining. We also constructed tetramers based on a series of mutated H-2K^d MHC I heavy chains, including H-2Kd-M1, H-2Kd-M2, and the dual mutant H-2Kd-M3. When compared to the WT tetramer, the three mutant tetramers stained a lower proportion of HBc87-95-specific CD8$^+$ T-cells within splenocytes from mice inoculated with peptide HBc87-95 ($0.31 \pm 0.06\%$, $0.30 \pm 0.05\%$, and $0.29 \pm 0.09\%$, respectively). These results indicated that mutations of the residues forming the salt bridge positioned over the peptide may impact specific-T-cell recognition.

3.4. The two different salt bridges formed by H-2K^d and HLA-B*4001

Though both H-2K^d and HLA-B*4001 contain the conserved negatively charged residue E163, the structures of these two MHC I molecules clearly display two different types of salt bridges over the N-terminus of their complexed peptides (Fig. 3). Compared to H-2K^d, the salt bridge of HLA-B*4001 is located closer to the N-terminus of the PBG, and an angle of ~30° can be observed between the positions of the two salt bridges. This is due to the different positively charged residues in the salt bridges of the two MHC I molecules. E163 of H-2K^d forms the salt bridge with residue R66, while the salt bridge of HLA-B*4001 is constructed by residues E163 and R62. We further investigated the Protein Data Bank (PDB) to determine whether there are other types of salt bridges in the previously determined MHC I structures. However, we only found the two types of salt bridges as in H-2K^d and HLA-B*4001, respectively. Rhesus macaque MHC I Mamu-B*17(PDB code:3RWE)and Mamu-B*098 (PDB code:4ZFZ) display the same salt bridge as H-2K^d, while the type of salt bridge in HLA-B*4001 is found in more MHC I molecules from mammals, such as Mamu-A*02 (PDB code: 3JTT), RT1-A1c (PDB code:1KJV), HLA-B*0702 (PDB code: 5EO0), HLA-B*2705 (PDB code: 1HSA), and HLA-B*4002 (PDB code: 5IEK).

However, in the structures of some MHC I available online thus far (*e.g.*, H-2L^d, H-2D^b, and H-2D^d), though they possess the same salt bridge-forming residues (R62 and E163) as HLA-B*4001, no salt bridge is formed (PDB codes: 1LD9, 1CE6, 1BII) (Supplemental Fig. S1). The "broken bridge" is also found in several HLA-B*2705 structures (*e.g.* PBD codes: 2BST and 1JGE) (Supplemental Fig. S1). Particularly, H-2D^d possesses both R62 and R66 in its α1 helix, but no salt bridge is formed
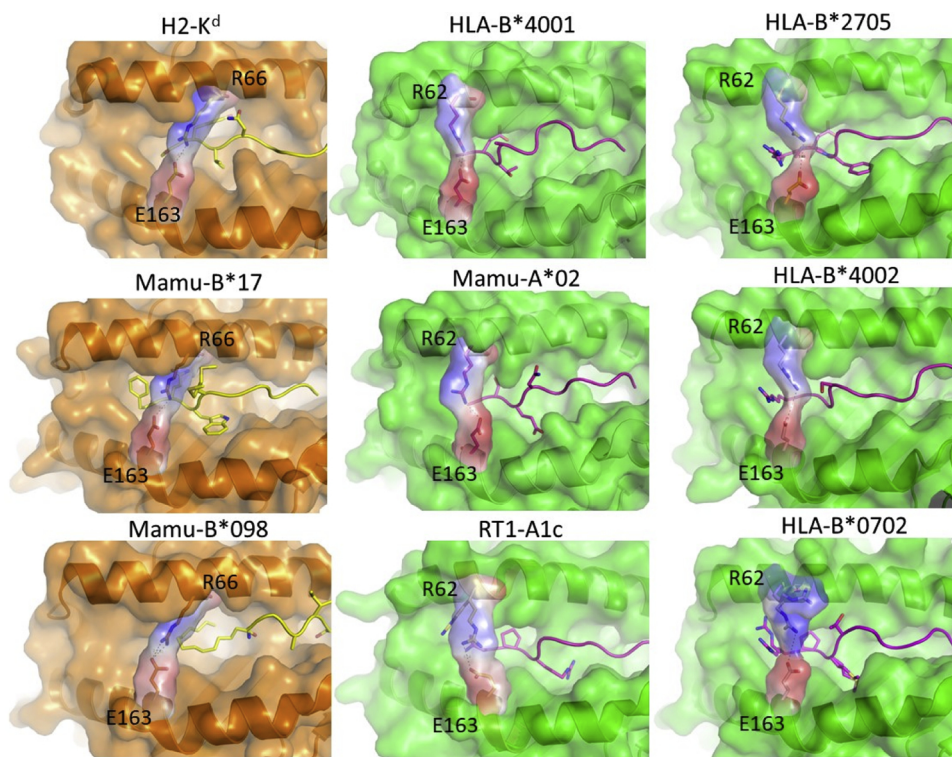
Fig. 3. Two different salt bridges in H-2K[d] and HLA-B*4001, as well as other MHC I molecules.

Mouse MHC I H-2K[d] possesses the Type 1 salt bridge formed by R66 and E163, shown as the vacuum electrostatic surface potential. Mamu-B*17 and Mamu-B*098 form the same type of salt bridge as H-2K[d]. Transparent surfaces of the α1 and α2 domains of these three MHC I molecules are shown in orange, while the presented peptides or lipopeptides are shown in yellow sticks. The Type 2 salt bridge is formed by R62 and E163, as in HLA-B*4001, and can also be found in Mamu-A*02, RT1-A1c, HLA-B*2705, HLA-B*4002, and HLA-B*0702. The α1 and α2 domains of these six MHC I molecules are shown in green transparent surfaces, while the peptides are shown in purple sticks. The black dashed lines in the structure represent the hydrogen bonds constructed by residues E163 and R66 (Type 1 salt bridge)/ R62 (Type 2 salt bridge). (For interpretation of the references to colour in this figure legend, the reader is referred to the web version of this article).

between E163 and either of these positively charged residues.

Next, we analyzed the hydrogen bonds within the two residues forming the salt bridge and the adjacent residues of both MHC I and the peptides (Fig. 4). Three different interactions contribute to the formation of the salt bridges: 1) the electrostatic interaction between R62 or R66 in the α1 helix and the E163 in the α2 helix. The hydrogen bonds constructed between residues R66 and E163 in H-2K[d] and between R62 and E163 in HLA-B*4001 are 2.59 Å and 2.75 Å, respectively. 2) R62 or R66 in the salt bridge can form a hydrogen bond with the carbonyl group of the P2 residue of the bound peptide in the PBG (as in both the H-2K[d] and HLA-B*4001 structures, and through a water molecule in Mamu-A*02). 3) For the MHC I-binding peptides with a hydrophilic residue at the P1 position, hydrogen bonds can be found between E163 and the side chains of the P1 residue of the peptide (as in the H-2K[d] structure but not HLA-B*4001) (Fig. 4). In HLA-B[*]4002 and HLA-B*0702, a water molecule links the interaction between R66 and E163 (Fig. 4). Further analysis indicated that this water molecule is conserved in a series of HLA-B*2705 structures (1UXS, 2A83, 2BSR, 3B6S, 3BP4, 1OF2, 1UXW, and 1W0W) (Supplemental Fig. S2).

We further analyzed the structures of H-2L[d], H-2D[b], and H-2D[d], which contain the same residues for salt bridge forming (R62 and E163) as HLA-B*4001 but do not contain salt bridges. In the MHC I H-2L[d], H-2D[b], and H-2D[d] structures, R62 is pulled away by E56 on the α1 helix, and R66 or K66 forms hydrogen bonds with E63 of the α1 helix. Thus, no salt bridge is formed in these three MHC I structures despite the fact that they contain the corresponding residues (Supplemental Fig. S3).

*3.5. Impact of the salt bridge on the structural conformations of MHC I and the bound peptide*

To investigate the potential influence of salt bridge formation on the structural conformation of the MHC/peptide complex, we superimposed the structures of the MHC I molecules with the two different salt bridges: R66-E163 (H-2K[d], Mamu-B*17, and Mamu-B*098) and R62-E163 (HLA-B*4001, Mamu-A*02, RT1-A1c, HLA-B*4002, HLA-B*0702, and HLA-B*2705) (Fig. 5A). Compared to the structure of MHC I with the R62-E163 salt bridge, the α2-helix of MHC I molecules with

the R66-E163 salt bridge has an conformational shift (approximately 1.65 Å between H-2K[d] and HLA-B*4001), using the α1-helix of MHC I as the benchmark during the alignment (Fig. 5B). The peptides in the structures of MHC I complexes with R66-E163 salt bridges also display conformational differences for the two residues at the P1 and P2 positions compared to the peptides under the R62-E163 salt bridges (Fig. 5C). The Cα of the P2 residues in the H-2K[d]-binding peptides are closer to the C-terminus of the PBG and located lower and closer to the bottom of the groove (Fig. 5D and 5E). The R66-E163 salt bridge acts as a "seatbelt" for the peptide, pushing both the conformational shift of the peptides and the α2-helices.

4. Discussion

Herein, we determined the crystal structures of HLA-B*4001 and H-2K[d] molecules with two representative different salt bridges spanning the presented peptides. Compared to WT, the peptide binding capacity of the salt bridge mutants was significantly lower. Meanwhile, the control mutants showed no statistical difference. Though the two salt bridges had distinct impacts on the conformational changes of the MHC I structures, both enhanced peptide binding and potentially contributed to TCR recognition.

Though the MHC I salt bridge-breaking mutants still bound to the peptides, their binding capacity were lower than WT. The impact on the thermostability of HLA-B*4001 by the mutants was not as much as that observed in the H-2K[d] mutants. This is may be due to the intrinsic features of different salt bridges in the two molecules. Using structural analysis, we found that the enhancement effect of peptide binding to MHC I was not only contributed by the direct formation of the salt bridge above the peptide main chain but also contributed by the conserved hydrogen bonds between the salt bridge-forming residues with the atoms on the main chain and the P1 residues of the peptides. A previous study indicates that a salt bridge (also called an ion pair in the study) formed by Argα80 and Aspβ57 in MHC class II heterodimers is also critical for surface expression and peptide presentation (Nalefski et al., 1995). However, unlike the salt bridge overhanging the MHC I peptide, this Argα80-Aspβ57 salt bridge is located under the main chain
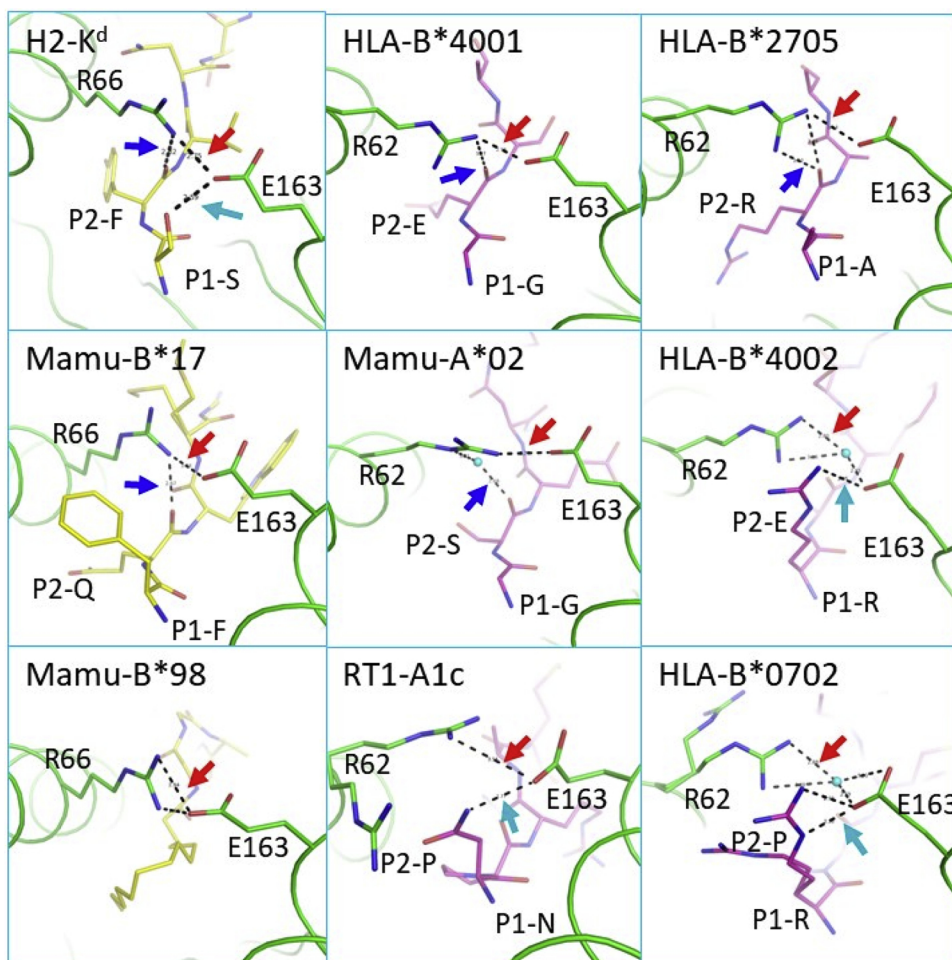
Fig. 4. The interactions between the two residues forming the salt bridge and the adjacent residues of both MHC I and the peptides.

The interactions between R66/R62 and E163 that form the salt bridge are denoted as red arrows. The cyan arrows represent the hydrogen bond between E163 and the side chains of the P1 residues of the peptides. The dark blue arrow marks the hydrogen bond between R62 or R66 and the carbonyl group of the P2 residue of the bound peptide in the PBG. In HLA-B*4002, HLA-B*0702 and Mamu-A*02, the cyan dots represent water molecules. The black dashed lines in the structures represent the hydrogen bonds. (For interpretation of the references to colour in this figure legend, the reader is referred to the web version of this article).
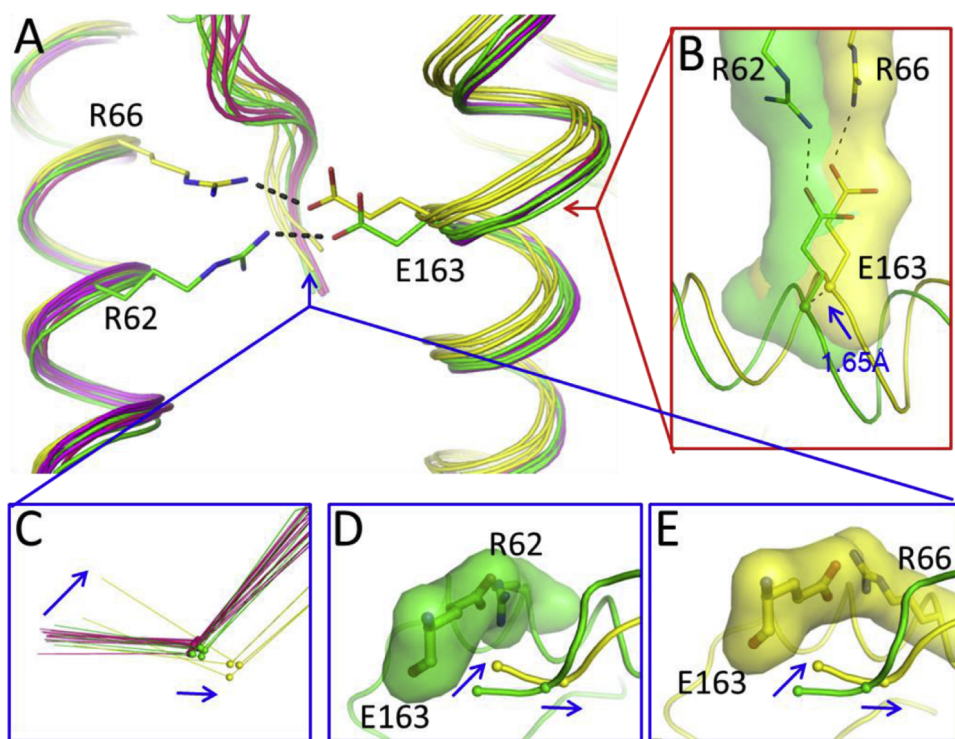
Fig. 5. The different influences on MHC I structural conformation by the two salt bridges. (**A**) Superimposed structures of MHC I molecules with two different salt bridges. The α1 and α2-helices of H-2K^d, Mamu-B*17, and Mamu-B*098 are shown as yellow, while the α1 and α2-helices of HLA-B*4001, Mamu-A*02, RT1-A1c, HLA-B*4002, HLA-B*0702, and HLA-B*2705 are green. The purple one indicates the different structures of B*2705. R66-E163 of H-2K^d and R62-E163 of HLA-B*4001 are denoted as yellow and green sticks, forming the salt bridge. (**B**) Using the α1-helix of MHC I as the benchmark, the α2-helix of H-2K^d with the R66-E163 salt bridge (yellow) is shifted ˜1.65 Å compared to the structure of HLA-B*4001 with the R62-E163 salt bridge (green). (**C**) Conformational difference of peptides in structures of MHC I complexes with R66-E163 and R62-E163 salt-bridges. Compared to peptides under the R62-E163 salt bridge, the residues in the P1 and P2 positions of peptides under the R66-E163 salt bridges have an obvious shift; the arrow represents the direction of displacement. (**D and E**) The Cα of the P2 residues of the H-2K^d-bound peptides (yellow) are closer to the C-terminus of the PBG compared to the R62-E163 salt bridge (green). (For interpretation of the references to colour in this figure legend, the reader is referred to the web version of this article).

of the MHC II-presented peptide and may contribute to P9 binding and the C-terminal hanging conformation of the MHC II-bound peptides.

The salt bridge above the peptide both enhances MHC I-peptide binding and contributes to TCR recognition of MHC I-peptide complexes. Birkinshaw et al. studied that a prototypical autoreactive BK6 TCR bound CD1a when the presented ligands were permissive. TCR docked over the A' roof of CD1a and a central CD1a salt-bridge network (Arg76-Glu154 salt-bridge) prevented the interaction between BK6 TCR and permissive ligands, and its autoreactivity was determined by contacts with CD1a. Nonpermissive ligands disrupted salt bridge interaction of CD1a, disrupt the properties of A' roof and could hinder engagement of hydrophobic CDR3β loop of the BK6 TCR with CD1a (Birkinshaw et al., 2015). Nurzia et al. indicate that the positive charging of Arg62 is preferred for the TCR recognition of Ankylosing Spondylitis-associated B*2705 complexes, as revealed by the R62 K and R62A mutants with an overall reduced capability to present peptides to CD8^{+} T-cells (Nurzia et al., 2012). Our data also demonstrate that T-cell recognition was significantly alleviated when we broke the MHC I salt bridge with R66A and E163A mutations. Previously determined complex structure between HLA-B*07:02 and KFJ37 TCR showed that both the R62 and E163 of HLA-B*07:02 can form hydrogen bonds with the residues in the CDR3α and CDR1α loops of the TCR, respectively (Chan et al., 2018). This indicated that the residues in the salt bridge can be directly-recognized by the TCR (Tynan et al., 2007). Meanwhile, our analysis also demonstrated that the salt bridge can lead to a conformational shift of the presented peptide and the relative locations of the α1 or α2 helices, which may subsequently and indirectly impact TCR recognition. Further structural studies are required to investigate the accurate and detailed recognition of MHC I/peptide complex containing the salt bridge by the TCR.

Nevertheless, our current study still has limitations. The mutant MHC I tetramers used in this study including the H-2K[d] mutants at R66 and/or E163A can dismantle the salt breakage and then may indirectly alter T cell response. However, these residues can also be recognized by TCR, thus, the mutation of these residues may also directly influence the TCR response. We cannot exclude the possibility that the altered T cell response was due to altered contacts with the mutated residues, rather than the loss of the salt bridge interaction.

In summary, our study indicates that the two different salt bridges in mammalian MHC I molecules, represented by HLA-B*4001 and H-2K[d], respectively, have different structural characteristics. And the mutations of the salt bridge-forming residues may impact both peptide binding and TCR recognition, directly or indirectly. Our data is helpful for the understanding of the CD8^{+} T-cell recognition of MHC I-presented peptides.

Appendix A. Supplementary data

Supplementary material related to this article can be found, in the online version, at doi:https://doi.org/10.1016/j.molimm.2019.06.005.

References

Baker, B.M., Scott, D.R., Blevins, S.J., Hawse, W.F., 2012. Structural and dynamic control of T-cell receptor specificity, cross-reactivity, and binding mechanism. Immunol. Rev. 250 (1), 10–31. https://doi.org/10.1111/j.1600-065X.2012.01165.x.

Birkinshaw, R.W., Pellicci, D.G., Cheng, T.Y., Keller, A.N., Sandoval-Romero, M., Gras, S., et al., 2015. Alphabeta T cell antigen receptor recognition of CD1a presenting self lipid ligands. Nat. Immunol. 16 (3), 258–266. https://doi.org/10.1038/ni.3098.

Bjorkman, P.J., Saper, M.A., Samraoui, B., Bennett, W.S., Strominger, J.L., Wiley, D.C., 1987. Structure of the human class I histocompatibility antigen, HLA-A2. Nature 329 (6139), 506–512. https://doi.org/10.1038/329506a0.

Borbulevych, O.Y., Piepenbrink, K.H., Gloor, B.E., Scott, D.R., Sommese, R.F., Cole, D.K., et al., 2009. T cell receptor cross-reactivity directed by antigen-dependent tuning of peptide-MHC molecular flexibility. Immunity 31 (6), 885–896. https://doi.org/10.1016/j.immuni.2009.11.003.

Chan, K.F., Gully, B.S., Gras, S., Beringer, D.X., Kjer-Nielsen, L., Cebon, J., et al., 2018. Divergent T-cell receptor recognition modes of a HLA-I restricted extended tumour-associated peptide. Nat. Commun. 9 (1), 1026. https://doi.org/10.1038/s41467-018-03321-w.

Fremont, D.H., Matsumura, M., Stura, E.A., Peterson, P.A., Wilson, I.A., 1992. Crystal structures of two viral peptides in complex with murine MHC class I H-2Kb. Science 257 (5072), 919–927.

Gras, S., Burrows, S.R., Turner, S.J., Sewell, A.K., McCluskey, J., Rossjohn, J., 2012. A structural voyage toward an understanding of the MHC-I-restricted immune response: lessons learned and much to be learned. Immunol. Rev. 250 (1), 61–81. https://doi.org/10.1111/j.1600-065X.2012.01159.x.

Hulsmeyer, M., Fiorillo, M.T., Bettosini, F., Sorrentino, R., Saenger, W., Ziegler, A., Uchanska-Ziegler, B., 2004. Dual, HLA-B27 subtype-dependent conformation of a self-peptide. J. Exp. Med. 199 (2), 271–281. https://doi.org/10.1084/jem.20031690.

Insaidoo, F.K., Borbulevych, O.Y., Hossain, M., Santhanagopolan, S.M., Baxter, T.K., Baker, B.M., 2011. Loss of T cell antigen recognition arising from changes in peptide and major histocompatibility complex protein flexibility: implications for vaccine design. J. Biol. Chem. 286 (46), 40163–40173. https://doi.org/10.1074/jbc.M111.283564.

Li, H., Zhou, M., Han, J., Zhu, X., Dong, T., Gao, G.F., Tien, P., 2005. Generation of murine CTL by a hepatitis B virus-specific peptide and evaluation of the adjuvant effect of heat shock protein glycoprotein 96 and its terminal fragments. J. Immunol. 174 (1), 195–204.

Liu, J., Dai, L., Qi, J., Gao, F., Feng, Y., Liu, W., et al., 2011. Diverse peptide presentation of rhesus macaque major histocompatibility complex class I Mamu-A 02 revealed by two peptide complex structures and insights into immune escape of simian immunodeficiency virus. J. Virol. 85 (14), 7372–7383. https://doi.org/10.1128/JVI.00350-11.

Liu, J., Qian, X., Chen, Z., Xu, X., Gao, F., Zhang, S., et al., 2012a. Crystal structure of cell adhesion molecule nectin-2/CD112 and its binding to immune receptor DNAM-1/CD226. J. Immunol. 188 (11), 5511–5520. https://doi.org/10.4049/jimmunol.1200324.

Liu, J., Zhang, S., Tan, S., Yi, Y., Wu, B., Cao, B., et al., 2012b. Cross-allele cytotoxic T lymphocyte responses against 2009 pandemic H1N1 influenza A virus among HLA-A24 and HLA-A3 supertype-positive individuals. J. Virol. 86 (24), 13281–13294. https://doi.org/10.1128/JVI.01841-12.

Madden, D.R., Garboczi, D.N., Wiley, D.C., 1993. The antigenic identity of peptide-MHC complexes: a comparison of the conformations of five viral peptides presented by HLA-A2. Cell 75 (4), 693–708.

Madden, D.R., Gorga, J.C., Strominger, J.L., Wiley, D.C., 1991. The structure of HLA-B27 reveals nonamer self-peptides bound in an extended conformation. Nature 353 (6342), 321–325. https://doi.org/10.1038/353321a0.

Mitaksov, V., Fremont, D.H., 2006. Structural definition of the H-2Kd peptide-binding motif. J. Biol. Chem. 281 (15), 10618–10625. https://doi.org/10.1074/jbc.M510511200.

Nalefski, E.A., Shaw, K.T., Rao, A., 1995. An ion pair in class II major histocompatibility complex heterodimers critical for surface expression and peptide presentation. J. Biol. Chem. 270 (38), 22351–22360.

Niu, L., Cheng, H., Zhang, S., Tan, S., Zhang, Y., Qi, J., et al., 2013. Structural basis for the differential classification of HLA-A*6802 and HLA-A*6801 into the A2 and A3 supertypes. Mol. Immunol. 55 (3–4), 381–392. https://doi.org/10.1016/j.molimm.2013.03.015.

Nurzia, E., Narzi, D., Cauli, A., Mathieu, A., Tedeschi, V., Caristi, S., et al., 2012. Interaction pattern of Arg 62 in the A-pocket of differentially disease-associated HLA-B27 subtypes suggests distinct TCR binding modes. PLoS One 7 (3), e32865. https://doi.org/10.1371/journal.pone.0032865.

Oh, H.L., Chia, A., Chang, C.X., Leong, H.N., Ling, K.L., Grotenbreg, G.M., et al., 2011. Engineering T cells specific for a dominant severe acute respiratory syndrome coronavirus CD8 T cell epitope. J. Virol. 85 (20), 10464–10471. https://doi.org/10.1128/JVI.05039-11.

Tan, S., Zhang, S., Wu, B., Zhao, Y., Zhang, W., Han, M., et al., 2017. Hemagglutinin-specific CD4(+) T-cell responses following 2009-pH1N1 inactivated split-vaccine inoculation in humans. Vaccine 35 (42), 5644–5652. https://doi.org/10.1016/j.vaccine.2017.08.061.

Tynan, F.E., Reid, H.H., Kjer-Nielsen, L., Miles, J.J., Wilce, M.C., Kostenko, L., et al., 2007. A T cell receptor flattens a bulged antigenic peptide presented by a major histocompatibility complex class I molecule. Nat. Immunol. 8 (3), 268–276. https://doi.org/10.1038/ni1432.

Xiao, J., Xiang, W., Chai, Y., Haywood, J., Qi, J., Ba, L., et al., 2016. Diversified anchoring features the peptide presentation of DLA-88*50801: first structural insight into domestic dog MHC class I. J. Immunol. 197 (6), 2306–2315. https://doi.org/10.4049/jimmunol.1600887.

Zhang, N., Qi, J., Feng, S., Gao, F., Liu, J., Pan, X., et al., 2011. Crystal structure of swine major histocompatibility complex class I SLA-1 0401 and identification of 2009 pandemic swine-origin influenza A H1N1 virus cytotoxic T lymphocyte epitope peptides. J. Virol. 85 (22), 11709–11724. https://doi.org/10.1128/JVI.05040-11.

Zhang, Y., Zhang, H., Ma, W., Liu, K., Zhao, M., Zhao, Y., et al., 2018. Evaluation of Zika Virus-specific T-cell responses in immunoprivileged organs of infected Ifnar1-/- mice. J. Vis. Exp. 140. https://doi.org/10.3791/58110.

Zhou, M., Xu, D., Li, X., Li, H., Shan, M., Tang, J., et al., 2006. Screening and identification of severe acute respiratory syndrome-associated coronavirus-specific CTL epitopes. J. Immunol. 177 (4), 2138–2145.

Zhou, M., Xu, Y., Lou, Z., Cole, D.K., Li, X., Liu, Y., et al., 2004. Complex assembly, crystallization and preliminary X-ray crystallographic studies of MHC H-2Kd complexed with an HBV-core nonapeptide. Acta Crystallogr. D Biol. Crystallogr. 60 (Pt 8), 1473–1475. https://doi.org/10.1107/S0907444904013587.